JACS
JOURNAL OF THE AMERICAN CHEMICAL SOCIETY
pubs.acs.org/JACS
Article

Scalable Design of Ru-Embedded Carbon Fabric Using Conventional Carbon Fiber Processing for Robust Electrocatalysts

Seok-Jin Kim,[#] Ga-Hyeun Lee,[#] Jung-Eun Lee, Javeed Mahmood, Gao-Feng Han, Inkyung Baek, Changbeom Jeon, Minjung Han, Hwakyung Jeong, Cafer T. Yavuz,* Han Gi Chae,* and Jong-Beom Baek*

Cite This: *J. Am. Chem. Soc.* 2024, 146, 13142−13150
Read Online

ABSTRACT: Metal−carbon composites are extensively utilized as electrochemical catalysts but face critical challenges in mass production and stability. We report a scalable manufacturing process for ruthenium surface-embedded fabric electrocatalysts (Ru-SFECs) via conventional fiber/fabric manufacturing. Ru-SFECs have excellent catalytic activity and stability toward the hydrogen evolution reaction, exhibiting a low overpotential of 11.9 mV at a current density of 10 mA cm^{-2} in an alkaline solution (1.0 M aq KOH solution) with only a slight overpotential increment (6.5%) after 10,000 cycles, whereas under identical conditions, that of commercial Pt/C increases 6-fold (from 1.3 to 7.8 mV). Using semipilot-scale equipment, a protocol is optimized for fabricating continuous self-supported electrocatalytic electrodes. Tailoring the fiber processing parameters (tension and temperature) can optimize the structural development, thereby achieving good catalytic performance and mechanical integrity. These findings underscore the significance of self-supporting catalysts, offering a general framework for stable, binder-free electrocatalytic electrode design.

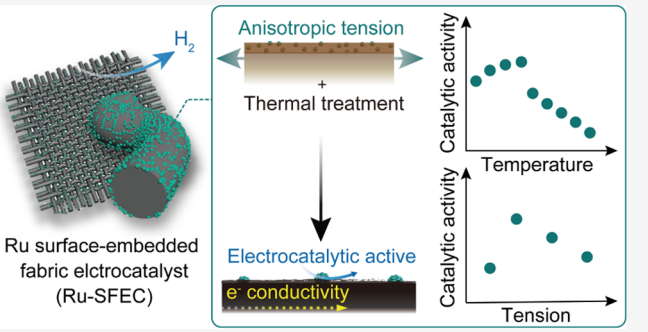

INTRODUCTION

Efficient and stable electrochemical catalysts have become increasingly important, owing to climate change and the energy crisis. The main challenge in energy conversion is designing an economical electrocatalytic electrode that is both efficient and stable. Developing a catalytic material is an important aspect of this effort; however, to complete the system, a suitable substrate material is also required to ensure stable performance.[1,2] This is because regardless of the excellence of the catalyst, if it adheres unreliably to the substrate (e.g., metal alloys, oxides, or carbon blacks), it can be detached easily; this may degrade the electrochemical performance.[3] To ensure substrate adherence, various techniques such as addition of binder(s), substrate functionalization, and thermal annealing have been used to improve the affinity between catalysts and substrates.[4−6] However, these techniques inevitably reduce the number of active sites, lowering the overall electrochemical performance.[7,8] The most reported catalytic systems for water splitting are carbon−metal nanocomposite powders, which are typically coated on an electrode using polymeric binders such as Nafion or polytetrafluoroethylene.[9,10] These binding polymers mask the electroactive sites, resulting in undesirable interfaces for electrons. In addition, constant gas evolution reactions and hydrogen bombardment can cause the coated materials to peel off when a high current density is repeatedly applied.[11,12] Therefore, designing a binder-free electrocatalyst is a critical prerequisite for durable and efficient electrocatalytic electrodes. Metal nanoparticles intertwined with carbon fibers (or fabrics) have recently drawn attention.[13,14] Diverse approaches for preparing carbon-fabric-based electrocatalytic electrodes have been reported, including hydrothermal synthesis, impregnation, and chemical vapor deposition.[15,16] However, most of these approaches yield a poor interface and are difficult to scale up to mass production. Hence, the development of a cost-effective and scalable manufacturing route for electrochemical electrodes with stable and high catalytic performance is of considerable interest.[10,11,17,18] Herein, we designed catalyst-embedded carbon fabric electrocatalysts using a conventional carbon fiber/fabric manufacturing process (Figure 1).

Ru, which operates more stably over a wider pH range than platinum, was selected as the active metal.[19,20] Polyacrylonitrile

Received: January 9, 2024
Revised: February 23, 2024
Accepted: March 27, 2024
Published: April 5, 2024

https://doi.org/10.1021/jacs.4c00332
J. Am. Chem. Soc. 2024, 146, 13142−13150

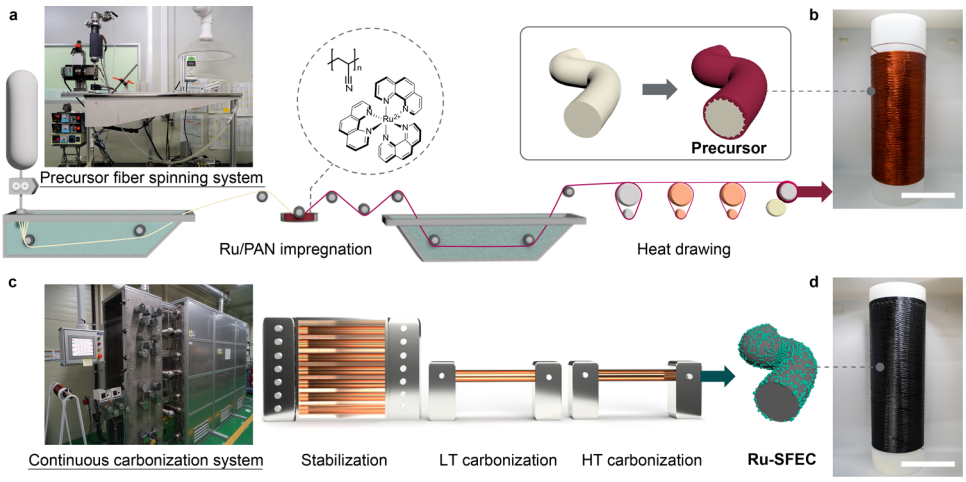

Figure 1. Schematic illustration of the ruthenium surface-embedded fabric electrocatalysts (Ru-SFEC) production. (a) Schematic of the setup used to produce continuous Ru-SFEC precursor fibers. (b) Spool of the Ru-SFEC precursor (scale bar: 10 cm). (c) Schematic of the continuous carbonization system for Ru-SFEC production composed of stabilization, low-temperature (LT), and high-temperature (HT) units. (d) Spool of Ru-SFEC (scale bar: 10 cm).

(PAN) was used as the carbon fiber precursor because of its widespread use in commercial carbon fiber production.[21]

RESULTS AND DISCUSSION

Synthesis of Ruthenium Surface-Embedded Fabric Electrocatalysts (Ru-SFECs). A polymeric precursor of Ru-SFEC was prepared in two consecutive steps (Figure 1). The as-spun PAN fibers were obtained via dry-jet wet spinning. The fibers were then passed through an impregnation bath containing a Ru-phenanthroline complex/PAN/dimethylformamide (DMF) solution and subjected to a drawing process.

To address the leaching issue of Ru during fiber processing, various metal chelating ligands were first evaluated based on the residual quantity of Ru and hydrophobicity probes of the ligand (Figure S1). Acetylacetonate inadequately mitigated Ru leaching, with a mere 5.0 wt % Ru uptake. In contrast, the anionic surfactant ligand, sodium oleate, had a superior uptake of 99.8 wt %; however, the long aliphatic carbon chain blocked the active catalytic sites, resulting in inferior electrocatalytic properties (24 mV at 10 mA cm^{-2}). Therefore, phenanthroline was selected to meet the requirement for both Ru retention (60.0 wt %) and catalytic activity.

Given the increased Laplace pressure on the curved fiber surfaces, the sheath layer experiences a high surface tension during coating. This could lead to an uneven distribution of the active elements around the fibers' periphery. Thus, the impregnation bath had an optimal solid concentration of 5 wt %, a Ru/ligand (phenanthroline) molar ratio of 1:3, and a Ru/PAN weight ratio of 1:2 for the fabrication of a precursor fiber with a uniformly coated sheath layer (143 ± 6 nm, Figure S2). The Ru-impregnated precursor fiber (Figures 1b and S3) was heat-treated using conditions typical for carbon fiber manufacturing (Figure 1c), while the high-temperature carbonization was undertaken in the temperature range 1200−2500 °C to trace the effect of structural development of carbon and catalytic Ru particles on electrochemical performance. The carbonized Ru-SFEC fiber (Figure 1d) exhibited sufficient processability for weaving into a fabric of area 3 × 3 cm^2 (Figure S4).

Characterization and Analysis of Ru-SFEC Structural Development: Heat Treatment, Conductivity, and Nanoparticle Formation. The structural development of Ru-SFEC was investigated in terms of heat treatment variables, including the carbonization temperature and applied stress. The migration of inner Ru atoms to the surface in Figure 2a represents the exsolution mechanism of the *in situ* growing Ru nanoparticles on the carbon backbone; this appears to originate from the Ru diffusion from the crystalline carbon to the surface. The internal structure of the fiber becomes more crystalline owing to the anisotropic stress applied to the fiber axis, which encourages the diffusion of imprisoned Ru to the fiber surface. Figure 2b shows the electrical conductivity and Ru residue as a function of the carbonization temperature (Figure S5). The electrical conductivity was measured by using a four-point probe (Figure S6). The electrical conductivity along the fiber axis increased in direct proportion to the formation and lengthening of the crystalline carbon basal planes. Interestingly, the Ru content (wt %) started to decline at temperatures above 1600 °C as the Ru particles were pushed to the surface owing to the carbon structure repacking and reduced surface energy between the metal particles and carbon structures. The electrical conductivity of the Ru-SFECs was in the range 132.93−257.07 S cm^{-1} (Table S1), which is more suitable to support electrochemical catalyst electrodes than that of other conductive carbon materials such as SWCNT/RGO fiber (20−102 S cm^{-1}),[22] aligned CNT/polymer (22−200 S cm^{-1}),[23] and polyethylene/CNT composite fiber (50 S cm^{-1}).[24] The temperature dependence of the structural development of Ru and carbon was investigated through X-ray diffraction (XRD) pattern analysis and transmission electron microscopy (TEM) (Figures 2c and S7). The patterns revealed that the crystal planes of hexagonal Ru, specifically the (100), (002), and (101) planes (marked with cyan lines), became prominent at 1600 °C, indicating crystal growth through Ostwald ripening.

The average Ru crystal size of 17.9 nm was calculated via the Scherrer equation using an XRD pattern at 1700 °C for carbonized Ru-SFEC, which is similar to the TEM observation (Figure S7). However, increasing the carbonization temperature to over 1800 °C decreased the crystallinity of the Ru particles as it approached the Ru melting point (2250 °C, Figure S8). Meanwhile, turbostratic carbon continuously

https://doi.org/10.1021/jacs.4c00332
J. Am. Chem. Soc. 2024, 146, 13142−13150

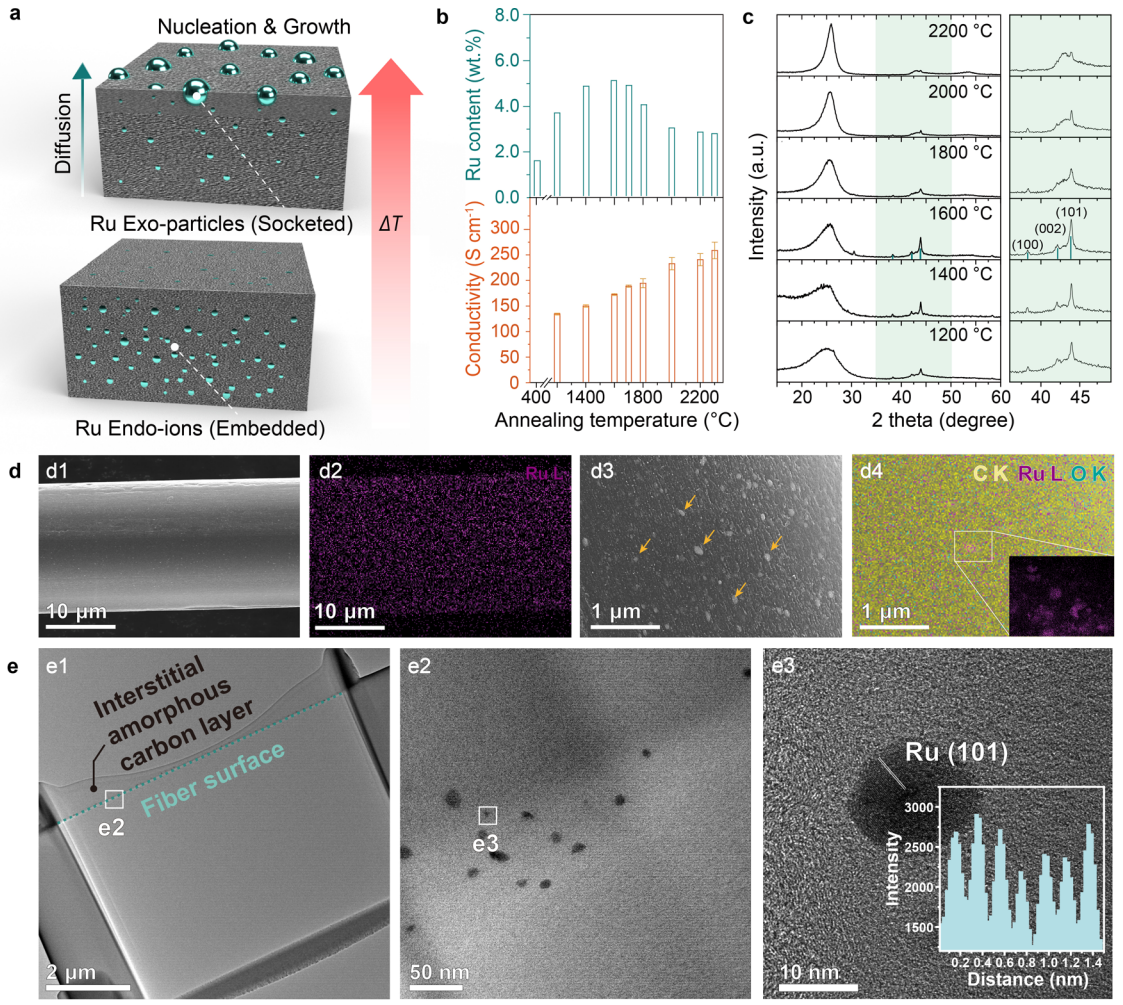

Figure 2. Microstructural analysis of Ru-SFEC with respect to the carbonization temperature. (a) Schematic of the exsolution mechanism of the temperature derived from active SFEC. (b) Graphs of the Ru content (top) derived via thermogravimetric analysis (TGA) of fiber in the air (10 °C min^{-1}) and electrical conductivities (bottom). (c) Powder XRD patterns with Ru peaks (Ru, PDF no. 89-4903, dark cyan bars). (d) Scanning electron microscopy (SEM) images in D1 at 1700 °C of carbonized Ru-SFEC; enlarged images of the particles in parts d3, d2, and d4 represent the corresponding energy-dispersive X-ray spectroscopy (EDS) maps of Ru. Violet dots indicate the Ru elements, and yellow dots denote the carbon elements. (e) TEM analysis at 1700 °C of heat-treated Ru-SFEC. (e1) Longitudinally sectioned fiber surface. The cyan dotted line represents the fiber surface. The inset shows the focused ion beam (FIB)-cut cross-sectional specimen. (e2, e3) Enlarged images of the Ru particle.

developed into a more graphitic structure as the carbonization temperature increased. At higher temperatures, the diameter of the carbonized fibers decreased, whereas the density increased, indicating that the structure was repacked because of the cross-linking of the ladder structure and lengthening and broadening of the carbon basal planes (Figure S9).

In Figure 2d, scanning electron microscopy (SEM) images (Figure 2d1,d3) and the corresponding energy-dispersive X-ray spectroscopy (EDS) mapping (Figure 2d2,d4) confirmed the presence of Ru on the fiber surface. The active material layer around the perimeter of each fiber strand exhibited a uniform coverage. The high-resolution transmission electron microscopy (HR-TEM) images of a thin fiber cross section prepared using a focused ion beam showed that highly crystalline Ru nanoparticles are selectively embedded at the surface (Figure 2e1,e2). The diameter of the Ru nanoparticles ranged from 5 to 18 nm. The inset *d*-spacing profile (Figure 2e3) exhibits a crystal lattice with an average spacing of approximately 0.21 nm, which corresponds to the (101) lattice planes of the Ru metal. The elemental maps also show homogeneous distributions of C, Ru, O, and N (Figures S2c,d and S10a–c). Given the strong atomic number contrast at these scattering angles, high-angle annular dark-field scanning transmission electron microscopy (HAADF–STEM) was used for single-atom imaging to detect electrons scattered through high angles (Figure S10d).

Correlating Tension on Ru-SFEC Microstructure and Nanoparticle Dynamics. The correlation between the applied tension and microstructure of Ru-SFEC is shown in Figure 3. The tension applied during carbonization is a significant factor in determining the molecular alignment of PAN polymer chains; it results in the preferred orientation of carbon crystallites along the fiber axis.[25,26] Notably, a region rich in Ru particles within the amorphous carbon phase can promote Ostwald ripening. In this context, the Tamman temperature of Ru (990 °C) enabled Ostwald ripening by modulating the diffusion of Ru atoms.[27] Consequently, as the temperature rose above the Tamman temperature, the diffusion rate of the Ru atoms accelerated, enabling the migration of Ru atoms from smaller particles to larger ones and leading to the growth and coarsening of the Ru particles. The Ru-SFEC fiber diameter also gradually decreased with an

https://doi.org/10.1021/jacs.4c00332
J. Am. Chem. Soc. 2024, 146, 13142−13150

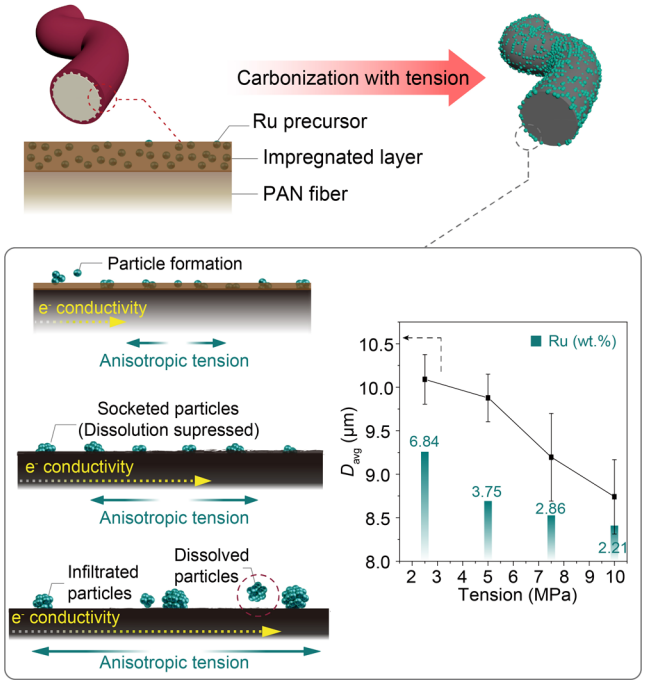

Figure 3. Schematic of tension-derived graphitic carbon structural development and Ru particle behavior. The application of the anisotropic tension restricts molecular chain relaxation, enhancing carbon structural density/orientation and contributing to Ru exsolution.

increase in the heat treatment temperature from 1200 to 1600 °C, which may have accelerated the progression of Ru particle exposure on the fiber surface above 1700 °C. The dissolution of the Ru particles also increased with a decreasing diameter. Furthermore, the Ru content decreased approximately 3-fold when the tension was increased from 2.5 to 10 MPa.

Two-dimensional wide-angle X-ray diffraction (WAXD) patterns of the faint diffraction intensity and the corresponding equatorial scan for carbon and Ru nanoparticles were used to observe the typical structural features of the Ru-SFEC fibers carbonized under different tensions (Figure 4a). Based on the full-width at half-maximum intensity obtained from the WAXD scan, the average crystallite dimensions L_c (perpendicular to the planes at the (002) peak) and L_a (in-plane at the[10] peak, detailed in Figure S11) were obtained using Bragg's law (Table S2).

Although all of the specimens exhibited similar *d*-spacings (0.344−0.345 nm), Ru-SFEC carbonized under a 5 MPa tension had larger carbon crystals than the other specimens. The orientation factor of the carbon was slightly reduced at 5 MPa, which may be interpreted as a distorted carbon crystallite confining the Ru nanoparticles.[28]

The development of the graphitic structure with respect to the tension variables was traced by combining average crystallite dimensions with the Raman spectroscopy results and mechanical properties (Figures 4b and S12). The ratios of I_D/I_G and I_A/I_G indicate the extent of the local disorder, particularly I_D/I_G, which is associated with the extent of graphitic crystallites and is related to the interdefect distance. I_D/I_G is also quantitatively correlated with L_a (consistent with the trend shown in Table S2). The slight variations in the I_{TPA}/I_G and I_A/I_G intensity ratios indicate a highly developed graphitic structure.

A tension value of 2.5 MPa is too low to control defect formation resulting from shrinkage during heat treatment. The fiber carbonized under 2.5 MPa tension had the second highest I_A/I_G and I_{TPA}/I_G ratio corresponding to the low values of L_a (10.06) and L_c (4.06), indicating loosened chain packing with the lowest tensile strength and tensile modulus. As the applied tension increased to 5 MPa, the shrinkage decreased and Ru distribution improved. Therefore, the ratio of disordered carbon structures was estimated to be the highest because of the influence of Ru. The advantageous distribution of the amorphous regions improved the dispersion of Ru. At 7.5 MPa, sp^3 bonds readily converted to sp^2 bonds, a graphitic structure developed, and the highest orientation factor and C(002) peak intensity were observed. Moreover, the structural density of the carbon increased, the metal was pushed into the amorphous region, and chain disorientation decreased. At 10 MPa, the orientation factor, L_a, tensile strength, and tensile modulus decreased significantly, owing to overstretching.

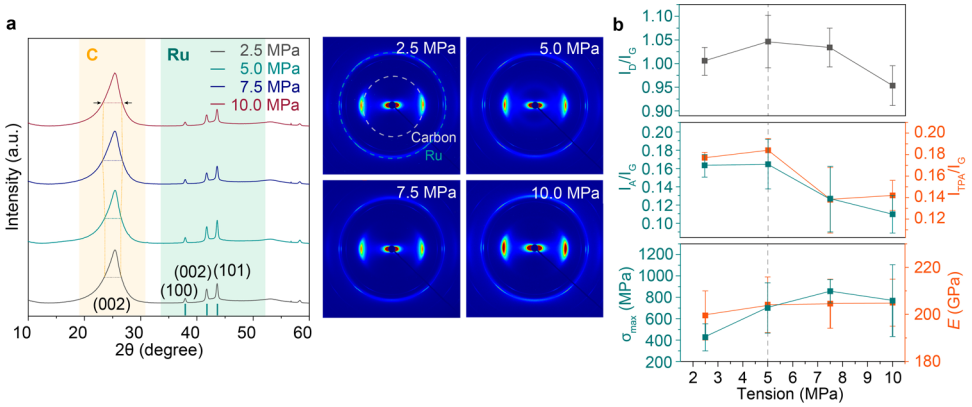

Figure 4. Microstructural analysis of Ru-SFEC with respect to the applied tension during carbonization. (a) Equatorial scans and two-dimensional (2D) WAXD patterns of Ru-SFEC carbonized at various tensions. PAN-based carbon fibers have two distinct diffraction fringes in the equatorial scan, namely, the crystal planes of (002) and (101). (b) Intensity ratio of the D and G bands (I_D/I_G, top) and A and G bands (I_A/I_G) with TPA and G bands (I_{TPA}/I_G, middle) in the Raman spectroscopy. The tensile stress of Ru-SFEC (σ_{max}, cyan) and Young's modulus (E, orange). The TPA band is attributed to a trans-polyacetylene-like structure. The well-known D and G bands could be attributed to the A_{1g} breathing mode vibration of the C_6 ring activated by defects and the E_{2g} vibration of the sp^2-bonded carbon pairs. The A band is assigned to a point vacancy structure. The A and D bands represent defects along the ab plane, whereas the G band indicates the graphitic order.

https://doi.org/10.1021/jacs.4c00332
J. Am. Chem. Soc. 2024, 146, 13142−13150

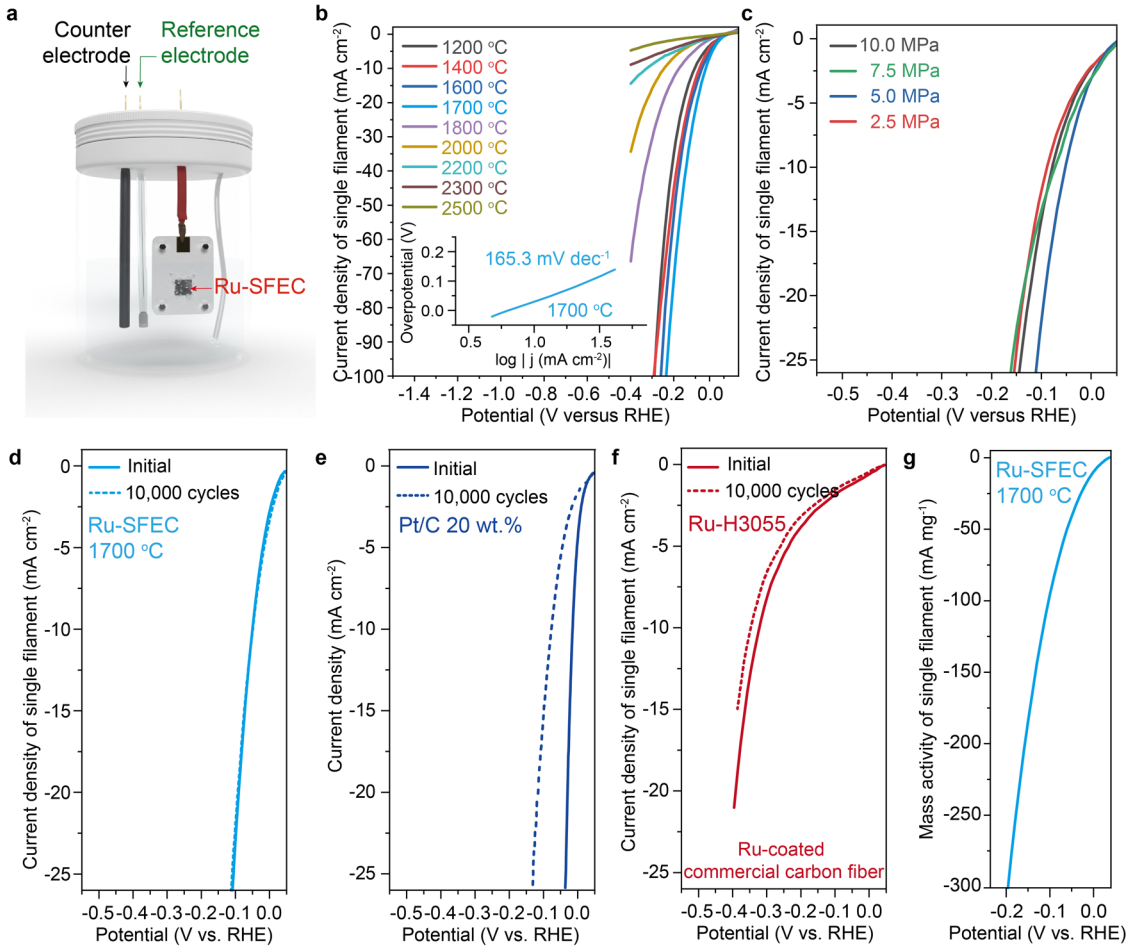

Figure 5. HER activity of Ru-SFECs varies with heat treatment temperature and applied tension, as shown in a comparative durability study. (a) Schematic illustration of the measurement system for electrocatalytic activity evaluation (1.0 M aq KOH). (b) Polarization curves (scan rate: 5 mV s^{-1}) of Ru-SFEC treated at different temperatures. (c) Polarization curves of Ru-SFEC carbonized under different applied tensions. (d–f) HER activity in an alkaline solution (1.0 M aq KOH) and polarization curves initially and after 10,000 cycles. (d) Carbonized Ru-SFEC at 1700 °C. (e) Commercial platinum on carbon (100 μg of Pt/C 20 wt %, powder). Powdery Pt/C was cast on a glassy carbon electrode. (f) Ru-coated commercial carbon fiber (Ru-H3055). (g) Mass activity at 1700 °C for carbonized Ru-SFEC.

The internal structure of the fiber under applied tension was monitored through X-ray photoelectron spectroscopy (XPS) to confirm the progress of carbonization and metal reduction (Ru^{n+} to Ru^0) (Figure S13). The N 1s peak started to disappear at 1200 °C; as the temperature increased, the C=C (284.42 eV) and C−C (285.57 eV) peaks were enhanced. The reduction in Ru^{n+} in the Ru 3d region was completed at approximately 1600 °C.

The correlative TEM Images reveal the Ru particle size distributions (Figure S14) as a function of the tension. The carbon backbone adopts a para-crystalline structure under high but feasible stress (7.5 MPa), which appears to affect the diffusion behavior of the Ru nanoparticles. The Ru nanoparticles were concentrated within the loosely structured amorphous carbon, where particles migrated from the crystalline graphitic layers. This migration led to sintering and exhibited a bimodal size distribution of 3−82 nm. A broadened Ru peak was also observed in the XRD data, revealing a wide Ru particle size distribution. Compared to other fibers in the 5−18 nm range, the 5.0 MPa tension-applied fiber with moderate orientation exhibited well-controlled Ru particle formation. A decrease in the Ru particle size is associated with a gradual increase in the concentration of the amorphous carbon phase during the development of the graphitic structure.

Based on the structural analysis, Ru-SFEC and conventional carbon fibers exhibit different structure development, owing to the inclusion of foreign Ru particles. While the conventional theory suggests that applying a maximum feasible tension enhances carbon fiber mechanical properties, this study finds that moderate tension is advantageous for electrocatalyst design. Adding Ru to the surface layer facilitates catalytic graphitization, thus reducing the temperature required to form a graphitic structure on the surface. However, Ru particles migrate toward the amorphous carbon region during heat treatment as the carbon crystalline structure develops, thus increasing the particle size. These Ru particles may contribute to surface flaws, such as cracks and disoriented graphitic crystals (Figure S15). The size of Ru particles increases with a higher carbonization temperature, tension, and heat treatment. Therefore, precisely controlling the processing parameters to optimize the delicate trade-off between the Ru particle dimensions and graphitic crystal plane orientation is imperative.

Electrocatalytic Performance of Ru-SFECs: Evaluating HER Activity, Durability, and Optimal Conditions. The

https://doi.org/10.1021/jacs.4c00332
J. Am. Chem. Soc. 2024, 146, 13142−13150

electrocatalytic activities of Ru-SFECs were examined through the change in current density (j, see Note S1 for the calculation of the current density) for the hydrogen evolution reaction (HER) using a fixture designed to evaluate the applicability of the Ru-SFECs as catalyst electrodes (Figure 5a). A graphite rod was used as the counter electrode, and Ag/AgCl was used as the reference electrode. The major factors affecting the catalytic activity were the electrical conductivity and the number of active sites on the fiber surface. An appropriate surface energy and thermal treatment temperature helped expose the active sites on the fiber surface. Ru-SFEC had the highest activity near 1700 °C, which is consistent with the structural analysis showing that Ru was exposed beyond 1600 °C (Figure 5b).

To ensure viable electrochemical properties in CF-based, self-supported electrocatalysts, two crucial aspects of microstructural development must be considered: (1) A well-defined crystalline carbon structure is vital for enabling electron mobility while inhibiting metal nanoparticle aggregation. The structure enhances conductivity and facilitates efficient electron transfer within the electrode material. (2) Exposed catalytic metal nanoparticles are essential for promoting the desired electrochemical reactions. Exposed nanoparticles facilitate the desired reactions by enabling efficient interactions between reactants and active sites on nanoparticle surfaces. Because Ru-SFEC under a tension of 5 MPa has an appropriate amorphous region to prevent aggregation and provide a uniform metal distribution, the HER performance with respect to the tension magnitude (Figure 5c) exhibits the highest activity at 5 MPa. Owing to the accumulation of the metal ejected from the graphitic crystal plane, the electrochemical starts to deteriorate from 7.5 to 10 MPa.

The primary feature of Ru-SFECs that sets them apart from commercial Pt/C and earlier self-standing electrocatalytic electrodes is their excellent durability (Figure 5d–f). The electrochemical HER revealed that Ru-SFECs have superior catalytic activity and exhibit a low overpotential of 11.9 mV at a current density of 10 mA cm^{-2} in an alkaline solution (1.0 M aq KOH solution) with excellent durability, maintain their original activity, surpass commercial Pt/C, and exhibit a slight overpotential increment of 6.5% after 10,000 cycles (Figure 5d). In contrast, Pt/C exhibits a 6-fold increase in overpotential (from 1.3 to 7.8 mV at a current density of 10 mA cm^{-2} after 10,000 cycles) (Figure 5e). To compare the effect of growing metals on the fiber structure, commercial carbon fiber (H3055, tensile strength of 800 ksi (T800), Hyosung Co.) was impregnated with Ru under the same conditions after polymer-sized materials and pollutants. The electrical conductivity of Ru-H3055 (170–216 S cm^{-1}) was lower than that of Ru-SFEC after annealing at 1700 °C (Table S1). The optimal temperature for Ru-H3055 was 1200 °C (Figure S16), which was lower than that for Ru-SFEC (1700 °C) because the internal structure of H3055 was already carbonized and the thermal energy was consumed only during Ru particle growth. However, the Ru particles found on preformed carbon fibers (Ru-H3055) have different interfaces that act with resistance and are not completely embedded, resulting in inferior activity and low stability (Figure 5f). Overall, the HER performance, activity (η; 129 mV at 100 mA cm^{-2}), and kinetics (165.3 mV dec^{-1}) of Ru-SFEC were similar to those reported for powdery-Ru nanocarbon composites such as Ru/C and Ru/CNT.[27] Furthermore, the fabric electrode exhibited excellent mass activity (Figure 5g).[29]

CONCLUSIONS

In this study, binder-free Ru-SFECs were developed using a conventional carbon fiber/fabric manufacturing process. The Ru-nanoparticle-embedded precursor was created via dry-jet wet spinning and subsequent heat treatment. We found that the fiber processing parameters, such as tension and heat treatment temperature, influenced the microstructural development, mechanical integrity, and catalytic performance of the electrodes. Using semipilot-scale equipment, a highly optimized protocol was established for fabricating continuous self-supported electrocatalytic electrodes. In contrast to previous methods, we improved the binding affinity by carbonizing catalyst-impregnated polymeric precursor fibers and weaving them into a fabric. The resulting electrode is flexible, lightweight, and suitable for various applications, including water electrolysis, wearable technology, and mobile devices, where weight is a constraint. This study lays a foundation for developing stable, binder-free, and flexible electrocatalytic electrodes. In addition, this technique holds potential for other catalytic reactions with different metals. Future research should focus on enhancing mechanical durability, electrical conductivity, and cost-effectiveness.

EXPERIMENTAL PROCEDURES

Materials. PAN with an average molecular weight of 150,000 g mol^{-1} and ruthenium(III) chloride were purchased from Sigma-Aldrich, Co. The PAN powders were pretreated in a vacuum oven at 80 °C for 1 day. Furthermore, 1,10-phenanthroline (>98.0%, high-performance liquid chromatography (HPLC)) was obtained from TCI Co. *N*,*N*-DMF (>99.9%, HPLC) was supplied by Samchun, Co. The commercial carbon fiber (H3055, tensile strength of 800 ksi) was purchased from Hyosung, Co

Preparation of Ru-Containing Sheath Solution. $RuCl_3$ (0.5 g) was dispersed in DMF (10 mL), after which 1,10-phenanthroline (phen, 1.32 g) was slowly added to the $RuCl_3$/DMF solution and stirred to form the $Ru(phen)_x$ complex. Vacuum-dried PAN powder (0.5 g) was dissolved in DMF (36.65 mL) using a magnetic stirrer with a stirring speed of 50 rpm at 60 °C. After the PAN dissolved, the solution became transparent, and the $Ru(phen)_x$ complex solution was slowly added. The resulting solution was stirred for 6 h (50 rpm, 60 °C). The solid concentration was 5 wt %, and the Ru content with respect to PAN was 50 wt %.

Preparation of PAN-Based Core Fiber. Vacuum-dried PAN powder (21 g) was dissolved in DMF (150 mL) by using an overhead mechanical stirrer with a stirring speed of 50 rpm at 60 °C for 12 h. The PAN fiber was dry-jet-wet-spun by using a custom-designed fiber spinning unit. Before spinning the fiber, the solution was degassed using a planetary centrifugal mixer at 1000 rpm for 5 min and thereafter at 2000 rpm for 10 min. The solution was maintained at 60 °C and extruded at 7.0 m min^{-1} through a spinneret (5 holes, 250 μm diameter/hole) into a coagulation bath (MeOH, 10 °C). The air gap between the spinneret and the coagulation bath was 10 mm. The fibers were collected using a take-up roller at 21.0 m min^{-1} (draw ratio of 3.0) from the washing bath (MeOH, 25 °C).

Impregnation of Ru-Containing Sheath on the PAN Fiber. The impregnation of the Ru-containing sheath layer was conducted during the postdrawing process. The unwound PAN fiber tow was passed through the impregnation bath at a speed of 3 m min^{-1}; the impregnation bath was filled with the Ru-containing sheath solution and three guide rollers ensured even distribution of the solution. Thereafter, the solution-impregnated fiber was introduced into a coagulation bath at 25 °C containing MeOH as the nonsolvent. Finally, the fiber tow was rolled up at a speed of 5 m min^{-1}. Two sequential heat rollers were employed after drawing, with temperatures set at 115 and 160 °C and speeds at 8 and 24 m min^{-1}, respectively (Figure 1a).

https://doi.org/10.1021/jacs.4c00332
J. Am. Chem. Soc. 2024, 146, 13142–13150

Impregnation of Ru-Containing Sheath on the Commercial Carbon Fiber. The commercial carbon fiber (H3055) was immersed in acetone for 12 h to remove polymer-sized compounds and pollutants. The desized carbon fiber was dried in a vacuum oven at 80 °C for 12 h. The commercial carbon fiber tow (12 k) was passed through an impregnation bath at 3 m min^{-1}; the bath was filled with the Ru-containing sheath solution and three guide rollers were used at 3 m min^{-1}. Thereafter, the Ru-containing sheath impregnated with H3055 was introduced into the coagulation bath (MeOH, 25 °C) as a nonsolvent. The fiber bundle was rolled up at a speed of 3 m min^{-1}.

Heat Treatment Conditions. All of the spun fibers were stabilized by heating at a rate of 3 °C min^{-1} to 260 °C and then maintained at 260 °C for 5 h under air to form a stable aromatic ladder structure with the linear PAN molecules. The stabilized fibers were then carbonized at 1200−2500 °C (Ru-SFEC) with a ramping rate of 4 °C min^{-1} under an Ar (99.999%) atmosphere. The 2.5−10 MPa stress was applied to fibers during stabilization and carbonization.

Electrochemical Measurements. The electrochemical studies were conducted on an electrochemical workstation (Ivium, The Netherlands) with a typical three-electrode cell. A graphite rod and a Ag/AgCl (saturated KCl) electrode were used as the counter and reference electrodes, respectively. For the powdery Pt/C test, 5 mg was introduced to a solution containing 20 μL of Nafion (a 5 wt % solution in a mix of lower aliphatic alcohol and water sourced from Aldrich Chemical, Inc.) and 1.0 mL of isopropyl alcohol. This mixture was subjected to ultrasonic agitation for 30 min in an ice-cooled environment to ensure a homogeneous catalyst ink. This ink was then carefully applied via drop casting onto a glassy carbon electrode to create a consistent film surface for subsequent electrochemical evaluation. All potentials were referenced with a reversible hydrogen electrode (RHE). Linear sweep voltammetry (LSV) was conducted using 1.0 M aq KOH solutions at a scan rate of 5 mV s^{-1}. All data were further used for the Ohmic drop (iR) correction. As the performance depended on the number of fibers, each single fiber filament was considered to be a cylindrical electrode when calculating the current density.

Preparation of HER Electrodes. For contact, a copper tape was attached to the handmade Teflon fixing plate, as shown in Figure 5a. The electrode area was obtained by assuming the shape of an elliptical cylinder and multiplying the number of fiber strands.

Conductivity Measurement. Ohm's law was used to calculate the electrical conductivity of a single filament carbon fiber after measuring the electrical resistivity using four-point probe equipment (CMT-SR1000N, Advanced Instrument Technology Co.) with a Jandel Engineering probe at 25 °C. Each specimen was prepared using the following methods to determine the electrical resistivity. First, a pure Ag source (99.99%) was deposited with specific patterns via thermal evaporation (Solar-Passage, DAEDONG High Technologies, Inc.) at an evaporation speed of 4 nm min^{-1} for 25 min on a UV−O_2 plasma-treated glass substrate for strong adhesion (140 W, 5 min, 60 sccm). The pattern was produced by using a custom-designed mask, as shown in Figure S6, to carry the electrical current. Second, the single filament was placed on the patterned region with a 2 mm gap. Third, the Ag paste (ELCOAT P-100, CANS) was placed only on the pattern in the area where the fiber was placed. Thereafter, four probes were applied to each circle at the end of the Ag pattern during the measurement process. The electrical resistivity of each fiber was evaluated as the average of at least 10 measurements. The electrical conductivity (σ) was calculated using eq 1.

$$\sigma = \frac{1}{R} \times \frac{L}{A} \tag{1}$$

where R, L, and A denote the electrical resistivity (Ω sq^{-1}), length between the probes (1 mm), and cross-sectional area of the fiber, respectively.

Instrumentation. Powder X-ray diffraction (PXRD) experiments were conducted with a high-power X-ray diffractometer D/MAX2500 V/PC (Cu Kα radiation, 40 kV, 200 mA, λ = 1.54056 Å) (Rigaku, Inc., Japan). Elemental analysis was conducted using a Flash 2000 Analyzer (Thermo Scientific, Inc.). TGA was conducted in air and nitrogen atmospheres at a ramping rate of 10 °C min^{-1} using an STA 8000 instrument (PerkinElmer, Inc.). XPS was conducted using an X-ray photoelectron spectrometer K-alpha (Thermo Fisher, Inc.). SEM and EDS images were taken with a SU7000 field emission scanning electron microscope (Hitachi Ltd., Japan) at 10 kV and 0.16 nA. HR-TEM and HAADF−STEM were performed using a JEM-2100F microscope (JEOL, Inc., Japan) at an operating voltage of 200 keV.

■ ASSOCIATED CONTENT

Data Availability Statement

The authors declare that data supporting the findings of this study are available within the article and the Supporting Information. All other data are available from the lead contact upon reasonable request.

Supporting Information

The Supporting Information is available free of charge at https://pubs.acs.org/doi/10.1021/jacs.4c00332.

Current density calculation method, Ru residue according to the metal−ligand, additional SEM, TEM, EDS images of Ru-SFECs, particle distribution of Ru in the fiber, photograph of the Ru-SFEC woven cloth and electrical conductivity measurement with data, phase diagram of C−Ru, diameter of Ru-SFEC from different tension, electrocatalytic activity of Ru−H3055 with respect to heat treatment temperature, XPS and Raman spectra of Ru-SFEC, TGA curves, orientation factor from WAXD, and supplementary figures for structural explanation (PDF)

■ AUTHOR INFORMATION

Corresponding Authors

Cafer T. Yavuz − *Advanced Membranes & Porous Materials Center (AMPMC), Physical Science & Engineering and KAUST Catalysis Center (KCC), Physical Science & Engineering, King Abdullah University of Science and Technology (KAUST), Thuwal 23955, Saudi Arabia;* orcid.org/0000-0003-0580-3331; Email: cafer.yavuz@kaust.edu.sa.

Han Gi Chae − *Department of Materials Science and Engineering, Ulsan National Institute of Science and Technology (UNIST), Ulsan 44919, Republic of Korea;* orcid.org/0000-0003-2196-0986; Email: hgchae@unist.ac.kr.

Jong-Beom Baek − *School of Energy and Chemical Engineering/Center for Dimension-Controllable Organic Frameworks (CDCOF), Ulsan National Institute of Science and Technology (UNIST), Ulsan 44919, Republic of Korea;* orcid.org/0000-0003-4785-2326; Email: jbbaek@unist.ac.kr.

Authors

Seok-Jin Kim − *School of Energy and Chemical Engineering/Center for Dimension-Controllable Organic Frameworks (CDCOF), Ulsan National Institute of Science and Technology (UNIST), Ulsan 44919, Republic of Korea; Advanced Membranes & Porous Materials Center (AMPMC), Physical Science & Engineering and KAUST Catalysis Center (KCC), Physical Science & Engineering, King Abdullah University of Science and Technology (KAUST), Thuwal 23955, Saudi Arabia;* orcid.org/0000-0002-6052-547X

Ga-Hyeun Lee − *Department of Materials Science and Engineering, Ulsan National Institute of Science and Technology (UNIST), Ulsan 44919, Republic of Korea*
Jung-Eun Lee − *Department of Materials Science and Engineering, Ulsan National Institute of Science and Technology (UNIST), Ulsan 44919, Republic of Korea;* orcid.org/0000-0003-2692-2356
Javeed Mahmood − *Advanced Membranes & Porous Materials Center (AMPMC), Physical Science & Engineering, King Abdullah University of Science and Technology (KAUST), Thuwal 23955, Saudi Arabia;* orcid.org/0000-0002-9159-3336
Gao-Feng Han − *Key Laboratory of Automobile Materials Ministry of Education, and School of Materials Science and Engineering, Jilin University, Changchun 130022, China;* orcid.org/0000-0001-5943-0492
Inkyung Baek − *Department of Materials Science and Engineering, Ulsan National Institute of Science and Technology (UNIST), Ulsan 44919, Republic of Korea*
Changbeom Jeon − *Department of Materials Science and Engineering, Ulsan National Institute of Science and Technology (UNIST), Ulsan 44919, Republic of Korea*
Minjung Han − *Department of Materials Science and Engineering, Ulsan National Institute of Science and Technology (UNIST), Ulsan 44919, Republic of Korea*
Hwakyung Jeong − *Department of Materials Science and Engineering, Ulsan National Institute of Science and Technology (UNIST), Ulsan 44919, Republic of Korea*

Complete contact information is available at: https://pubs.acs.org/10.1021/jacs.4c00332

Author Contributions

[#]S.-J.K. and G.-H.L. contributed equally to this work.

Funding

This research was supported by the Creative Research Initiative (CRI, RS-2023-00221668) and Basic Science Research Programs (2021R1A6A3A03039501 and 2021R1A2C2004404) through the National Research Foundation (NRF) of Korea, funded by the Ministry of Science, ICT (MSIT) and the Ministry of Education.

Notes

The authors declare no competing financial interest.
Resource Availability Further information and requests for resources should be directed to and will be fulfilled by the lead contact, Han Gi Chae (hgchae@unist.ac.kr).
Materials availability This study did not generate new unique reagents.

■ ACKNOWLEDGMENTS

The WAXD experiments were performed in the PAL beamline (6D C&S UNIST-PAL).

■ ABBREVIATIONS

PAN, polyacrylonitrile; DMF, dimethylformamide; XRD, X-ray diffraction; TEM, transmission electron microscopy; SEM, scanning electron microscopy; EDS, energy-dispersive X-ray spectroscopy; HR-TEM, high-resolution transmission electron microscopy; HAADF−STEM, high-angle annular dark-field scanning transmission electron microscopy; WAXD, wide-angle X-ray diffraction; XPS, X-ray photoelectron spectroscopy; HER, hydrogen evolution reaction

■ REFERENCES

(1) Dai, Y.; Lu, P.; Cao, Z.; Campbell, C. T.; Xia, Y. The physical chemistry and materials science behind sinter-resistant catalysts. *Chem. Soc. Rev.* **2018**, *47*, 4314−4331.
(2) Liu, J.; Zhu, D.; Zheng, Y.; Vasileff, A.; Qiao, S.-Z. Self-supported earth-abundant nanoarrays as efficient and robust electrocatalysts for energy-related reactions. *ACS Catal.* **2018**, *8*, 6707−6732.
(3) Mazloomi, S. K.; Sulaiman, N. Influencing factors of water electrolysis electrical efficiency. *Renewable Sustainable Energy Rev.* **2012**, *16*, 4257−4263.
(4) Wang, P. C.; Wang, B. G. Interface engineering of binder-free earth-abundant electrocatalysts for efficient advanced energy conversion. *ChemSusChem* **2020**, *13*, 4795−4811.
(5) Chanda, D.; Hnát, J.; Paidar, M.; Schauer, J.; Bouzek, K. Synthesis and characterization of NiFe2O4 electrocatalyst for the hydrogen evolution reaction in alkaline water electrolysis using different polymer binders. *J. Power Sources* **2015**, *285*, 217−226.
(6) Parvin, S.; Kumar, A.; Ghosh, A.; Bhattacharyya, S. An earth-abundant bimetallic catalyst coated metallic nanowire grown electrode with platinum-like pH-universal hydrogen evolution activity at high current density. *Chem. Sci.* **2020**, *11*, 3893−3902.
(7) Bernsmeier, D.; Chuenchom, L.; Paul, B.; Rümmler, S.; Smarsly, B.; Kraehnert, R. Highly active binder-free catalytic coatings for heterogeneous catalysis and electrocatalysis: Pd on mesoporous carbon and its application in butadiene hydrogenation and hydrogen evolution. *ACS Catal.* **2016**, *6*, 8255−8263.
(8) Kashale, A. A.; Yi, C. H.; Cheng, K. Y.; Guo, J. S.; Pan, Y. H.; Chen, I. W. P. Binder-free heterostructured NiFe2O4/NiFe LDH nanosheet composite electrocatalysts for oxygen evolution reactions. *ACS Appl. Energy Mater.* **2020**, *3*, 10831−10840.
(9) Chandrasekaran, S.; Khandelwal, M.; Dayong, F.; Sui, L.; Chung, J. S.; Misra, R. D. K.; Yin, P.; Kim, E. J.; Kim, W.; Vanchiappan, A.; Lui, Y.; Hur, S. H.; Zhang, H.; Bowen, C. Developments and perspectives on robust nano- and microstructured binder-free electrodes for bifunctional water electrolysis and beyond. *Adv. Energy Mater.* **2022**, *12*, No. 2200409.
(10) Yang, H.; Driess, M.; Menezes, P. W. Self−supported electrocatalysts for practical water electrolysis. *Adv. Energy Mater.* **2021**, *11*, No. 2102074.
(11) Ma, T. Y.; Dai, S.; Qiao, S. Z. Self-supported electrocatalysts for advanced energy conversion processes. *Mater. Today* **2016**, *19*, 265−273.
(12) Xue, Y.; Hui, L.; Yu, H.; Liu, Y.; Fang, Y.; Huang, B.; Zhao, Y.; Li, Z.; Li, Y. Rationally engineered active sites for efficient and durable hydrogen generation. *Nat. Commun.* **2019**, *10*, No. 2281.
(13) Chen, S.; Qiu, L.; Cheng, H.-M. Carbon-based fibers for advanced electrochemical energy storage devices. *Chem. Rev.* **2020**, *120*, 2811−2878.
(14) Zhu, C.; Usiskin, R. E.; Yu, Y.; Maier, J. The nanoscale circuitry of battery electrodes. *Science* **2017**, *358*, No. eaao2808, DOI: 10.1126/science.aao2808.
(15) Koutavarapu, R.; Reddy, V.; Babu, B.; Reddy, K. R.; Cho, M.; Shim, J. Carbon cloth/transition metals-based hybrids with controllable architectures for electrocatalytic hydrogen evolution - A review. *Int. J. Hydrogen Energy* **2020**, *45*, 7716−7740.
(16) Wang, J.; Cui, W.; Liu, Q.; Xing, Z.; Asiri, A. M.; Sun, X. Recent progress in cobalt-based heterogeneous catalysts for electrochemical water splitting. *Adv. Mater.* **2016**, *28*, 215−230.
(17) Liu, Z.; Zhao, Z.; Wang, Y.; Dou, S.; Yan, D.; Liu, D.; Xia, Z.; Wang, S. In situ exfoliated, edge-rich, oxygen-functionalized graphene from carbon fibers for oxygen electrocatalysis. *Adv. Mater.* **2017**, *29*, No. 1606207.
(18) Han, X.; Wu, X.; Deng, Y.; Liu, J.; Lu, J.; Zhong, C.; Hu, W. Ultrafine Pt nanoparticle-decorated pyrite-type CoS2 nanosheet arrays coated on carbon cloth as a bifunctional electrode for overall water splitting. *Adv. Energy Mater.* **2018**, *8*, No. 1800935.
(19) Li, C.; Baek, J.-B. Recent advances in noble metal (Pt, Ru, and Ir)-based electrocatalysts for efficient hydrogen evolution reaction. *ACS Omega* **2020**, *5*, 31−40.

(20) Kweon, D. H.; Okyay, M. S.; Kim, S.-J.; Jeon, J.-P.; Noh, H.-J.; Park, N.; Mahmood, J.; Baek, J.-B. Ruthenium anchored on carbon nanotube electrocatalyst for hydrogen production with enhanced Faradaic efficiency. *Nat. Commun.* **2020**, *11*, No. 1278.
(21) Newcomb, B. A. Processing, structure, and properties of carbon fibers. *Composites, Part A* **2016**, *91*, 262−282.
(22) Yu, D.; Goh, K.; Wang, H.; Wei, L.; Jiang, W.; Zhang, Q.; Dai, L.; Chen, Y. Scalable synthesis of hierarchically structured carbon nanotube-graphene fibres for capacitive energy storage. *Nat. Nanotechnol.* **2014**, *9*, 555−562.
(23) Peng, H. S. Aligned carbon nanotube/polymer composite films with robust flexibility, high transparency, and excellent conductivity. *J. Am. Chem. Soc.* **2008**, *130*, 42−43.
(24) Zhang, S. J.; Lin, W.; Wong, C. P.; Bucknall, D. G.; Kumar, S. Nanocomposites of carbon nanotube fibers prepared by polymer crystallization. *ACS Appl. Mater. Interfaces* **2010**, *2*, 1642−1647.
(25) Chae, H. G.; Kumar, S. Making strong fibers. *Science* **2008**, *319*, 908−909.
(26) Fox, B. Making stronger carbon-fiber precursors. *Science* **2019**, *366*, 1314−1315.
(27) Bae, S.-Y.; Mahmood, J.; Jeon, I.-Y.; Baek, J.-B. Recent advances in ruthenium-based electrocatalysts for the hydrogen evolution reaction. *Nanoscale Horiz.* **2020**, *5*, 43−56.
(28) Morton, W. E.; Hearle, J. W. S. *Physical Properties of Textile Fibres*, 4th ed.; Morton, W. E.; Hearle, J. W. S., Eds.; Woodhead Publishing, 2008; Vol. *1*−*81*, pp 559−624.
(29) Cao, X.; Huo, J.; Li, L.; Qu, J.; Zhao, Y.; Chen, W.; Liu, C.; Liu, H.; Wang, G. Recent advances in engineered Ru-based electrocatalysts for the hydrogen/oxygen conversion reactions. *Adv. Energy Mater.* **2022**, *12*, No. 2202119.

https://doi.org/10.1021/jacs.4c00332
J. Am. Chem. Soc. 2024, 146, 13142−13150